Light-Scattering Study on Porous Membrane Formation by Dry-Cast Process

Hideto Matsuyama, Masanori Tachibana, Taisuke Maki, Masaaki Teramoto

Department of Chemistry and Materials Technology, Kyoto Institute of Technology, Matsugasaki, Sakyo-ku, Kyoto 606-8585, Japan

Received 17 October 2001; accepted 3 January 2002

ABSTRACT: The phase-separation mechanism during porous membrane formation by the dry-cast process was investigated by the light-scattering method in poly(methyl methacrylate)/ethyl acetate (EA)/2-methyl-2,4-pentanediol system. The evaporation of EA from the cast solution induced the phase separation and thus the porous membrane was obtained. By the light-scattering measurement on the phase-separation kinetics, the phase separation was found to occur by a spinodal decomposition mechanism. As the amount of nonsolvent in the cast solution decreased, the structure growth rate decreased and the growth stopped soon. The obtained porous structure was isotropic rather than asymmetric. The average interpore distances obtained from the SEM observation roughly agreed with the final constant interphase periodic distances measured by the light-scattering method. © 2002 Wiley Periodicals, Inc. J Appl Polym Sci 86: 3205–3209, 2002

Key words: phase separation; light scattering; microporous membrane; dry-cast process; spinodal decomposition; poly(methyl methacrylate)

INTRODUCTION

The majority of porous membranes are prepared by phase separation of polymer solutions. The phase-separation methods can be classified into main four processes: thermally induced phase separation (TIPS), air-casting (dry-casting) of a polymer solution, precipitation from the vapor phase, and immersion precipitation.[1] In the latter three processes, the phase separation is induced by the presence of nonsolvents. A ternary system of polymer, solvent, and nonsolvent is normally treated in the nonsolvent-induced phase-separation process. Undoubtedly, both thermodynamic study on the three-component phase diagram and kinetic study on the change of composition during the membrane formation are essential to control the membrane structure. The phase diagram of the ternary system has been well understood.[2,3] The crystallization isotherms as well as the binodal envelopes were calculated in crystalline polymers.[4–6] The changes of composition paths during the membrane formation were analyzed based on many mass-transfer models.[7–10] Although these models are strictly correct until the occurrence of phase separation, the information about the composition paths can tell us the types of the phase separation such as spinodal decomposition (SD) and nucleation and growth (NG).

Surprisingly, in the membrane-formation process, few studies reported on the kinetics of the phase separation itself. Nunes and Inoue investigated the phase-separation mechanism during the membrane formation in the immersion precipitation method by light scattering.[11] They found the conditions for the SD or NG mechanism. Barth et al. identified the mechanism of phase inversion with light-scattering experiments in the formation of polysulfone and polyethersulfone membranes.[12] Recently, Schuhmacher et al. investigated the liquid–liquid phase-separation mechanism via NG by light scattering and determined the growth constants in different component concentrations.[13]

In our previous study, the phase-separation mechanism in the dry-cast process was studied in the cellulose acetate/dimethylformamide (DMF)/2-methyl-2,4-pentanediol (MPD) system.[14] Phase separation occurred by SD when the path of composition change resulting from the evaporation of DMF was close to the critical point. Characteristic properties of the early stage of SD such as an apparent diffusion coefficient and an interface periodic distance were obtained.

As far as we know, the growth of the phase-separated structure in the intermediate or later stage of SD has not yet been investigated by light scattering in the membrane-formation process. The purpose of this work was to clarify such growth behavior in phase separation in the dry-cast process.

Correspondence to: H. Matsuyama (matsuyama@chem.kit.ac.jp).

Journal of Applied Polymer Science, Vol. 86, 3205–3209 (2002)

EXPERIMENTAL

Materials

The polymer was poly(methyl methacrylate) (PMMA; secondary standard, M_w = 102,600, M_n = 48,300; Aldrich Chemical Co., Milwaukee, WI). The solvent and nonsolvent were ethyl acetate (EA, bp: 350 K; Wako Pure Chemicals, Osaka, Japan) and 2-methyl-2,4-pentanediol (MPD, bp: 470 K; Wako Pure Chemicals), respectively.

Cloud point curve

Homogeneous polymer solutions with several polymer concentrations were prepared at 298 K. The polymer solution already contained adequate amounts of nonsolvent. Then, a small amount of nonsolvent was successively added to the solution. The cloud point was determined visually by noting the appearance of turbidity.

Membrane preparation

Homogeneous dope solutions were initially prepared. The polymer concentration in the dope solution was fixed at 15 wt % and the nonsolvent concentration was changed. Polymer and nonsolvent weight percentages in the dope solution are abbreviated as P and N, respectively (e.g., P15N25 means 15 wt % of polymer and 25 wt % of nonsolvent). The dope solution was cast onto the glass plate to a 254-μm clearance gap and the film was put on the balance placed in the chamber, where temperature and humidity were set at 298 K and less than 20%, respectively. The evaporation of EA induced the phase separation of the polymer solution and the film became opaque. Because the boiling point of EA is much lower than that of MPD, only EA was evaporated in the initial stage. Thus, the film weight decreased initially and then became nearly constant. After obtaining the constant weight, the film was immersed in 50 wt % aqueous methanol solution to extract MPD from the membrane.

The membrane was freeze-dried for the SEM observation. The dry membrane was immersed in liquid nitrogen, fractured, and coated with Au/Pd. The cross section was viewed by an S-800 scanning electron microscope (Hitachi, Tokyo, Japan) under an accelerating voltage of 15 kV.

Light-scattering measurement

To measure the phase separation rate, the light-scattering experiment was carried out by a DYNA-3000 polymer dynamics analyzer (Otsuka Electronics Co., Japan). The polymer solution cast onto the glass plate was located between the light source and the detector. The measurement was done at a room temperature of 294–297 K and under a relative humidity of 21–35%. The light scattering attributed to the phase separation brought about by the evaporation of EA was followed at the time interval of 1 s.

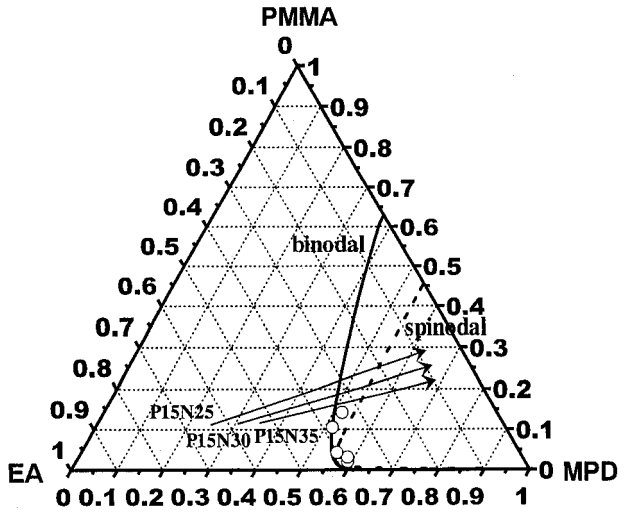

Figure 1 Phase diagram and paths of composition change during the membrane formation. Solid line: binodal curve; dotted line: spinodal curve; ○: cloud point.

RESULTS AND DISCUSSION

Figure 1 shows the phase diagram. The open circles in this figure denote the experimental data of the cloud point. In this system, a large amount of nonsolvent is necessary to induce the phase separation. For example, when the polymer volume percentage is 10%, more than 50% of nonsolvent is necessary for the phase separation. Gibbs' free energy of mixing for the ternary system ΔG_m is expressed as eq. (1), based on Flory–Huggins theory.[15]

$$\Delta G_m/RT = n_1\ln\phi_1 + n_2\ln\phi_2 + n_3\ln\phi_3 + g_{12}n_1\phi_2 + g_{13}n_1\phi_3 + g_{23}n_2\phi_3 \quad (1)$$

Here, subscripts 1, 2, and 3 denote nonsolvent, solvent, and polymer, respectively; n_i and ϕ_i are the number of moles and the volume fraction of component i; g_{ij} is the interaction parameter between component i and j. By using ΔG_m, binodal and spinodal lines can be calculated if values of g_{ij} are known.[2] The interaction parameter g_{13} was determined as 0.92 from the swelling experiment.[16] The solvent–polymer interaction parameter g_{23} was estimated by the solubility parameter difference.[17] The estimated value was 0.35. When the value of 1.40 was used for g_{12}, the binodal line agreed with the cloud point data, as shown in Figure 1. The calculated spinodal line is shown in Figure 1 as a dotted line.

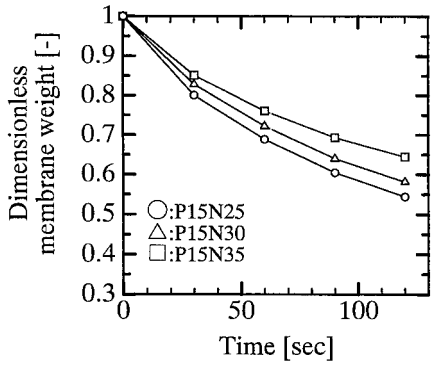

Figure 2 Weight change during the solvent evaporation process.

Because the boiling point of EA (350 K) is much lower than that of MPD (470 K), we can assume that only EA evaporates during the phase separation. Under this assumption, the composition of the polymer solution will change on the straight line, connecting a point of initial composition to a point of pure solvent. Initial compositions in the cast solutions used in this work were P15N25, P15N30, and P15N35. The paths of the composition change in the respective cases are shown in Figure 1 as arrows.

Figure 2 shows the weight change during the membrane-formation process. The ordinate is the dimensionless membrane weight, which is defined as the weight after evaporation divided by the initial weight. As the weight percentage of N in the cast solution decreased, the solution weight decreased a little faster because of the increase of the amount of the volatile solvent. This means that the composition change to the direction shown as arrows in Figure 1 occurs faster in the low N condition. However, the difference is not so remarkable.

Figure 3 shows the light-scattering results in P15N35. The scattered intensity I_s showed the maximum, which indicates that the phase separation occurred not by the nucleation and growth (NG) mechanism but by the spinodal decomposition (SD) mechanism.[11] As time passes, the location of the maximum of I_s was shifted to the lower scattered angle region. This was attributable to the growth of the structure.

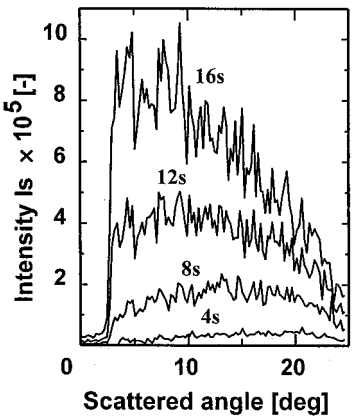

Figure 3 Relation between the scattered light intensity I_s and the scattered angle in P15N35.

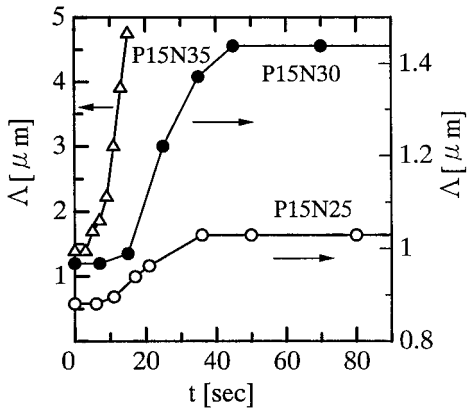

Figure 4 Time courses of the interphase periodic distance Λ.

The interphase periodic distance Λ can be related to the scattered angle θ, where I_s shows the maximum, by eq. (2):

$$\Lambda = \frac{\lambda_0}{2n_0 \sin(\theta/2)} \tag{2}$$

Here n_0 is the solution refractive index and λ_0 is the wavelength *in vacuo* (633 nm). The time courses of Λ are shown in Figure 4. In all three cases, Λ was initially constant, then increased, and finally became constant again except for the P15N35 solution. In P15N35, the scattered angle, where I_s showed maximum, was shifted to the low value and the maximum of I_s disappeared, as shown in Figure 3. The region of initial constant Λ corresponds to the early stage of SD. In the early stage of SD, the growth rate of the concentration fluctuation $R(q)$ can be related to a wavenumber q [$= 4\pi n_0/\lambda_0 \sin(\theta/2)$] as expressed in the following equation[18,19]:

$$R(q)/q^2 = D_{\text{app}}(1 - q^2/2q_m^2) \tag{3}$$

where D_{app} is the apparent diffusion coefficient and q_m is the wavenumber of maximum scattered light intensity.

Figure 5 shows the plot of $R(q)/q^2$ versus q^2. The obtained linear relations in three cases are in accordance with the expectation of eq. (3). The intercepts of the straight lines give D_{app}. The values of D_{app} are summarized in Table I together with the polymer concentration at which the composition change path crosses the spinodal line in Figure 1. D_{app} depends on both thermodynamic and kinetic aspects.[11] For instance, D_{app} is higher when the self-diffusion coeffi-

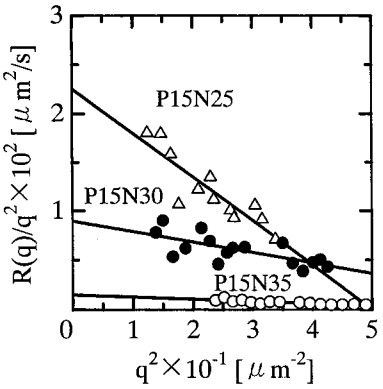

Figure 5 Relation between $R(q)/q^2$ and q^2.

cient of polymer is higher and the quench depth (distance from the spinodal line) is deeper. As N in the cast solution increased, D_{app} increased as a result of the higher self-diffusion coefficient brought about by the decrease of the polymer concentration shown in Table I.

As can be seen in Figure 4, the growth rate of Λ increased concomitantly with the increase of N. Generally, the growth of Λ is promoted when the continuous (matrix) phase viscosity is low and the volume fraction of the droplet phase is large.[20,21] One reason for the higher growth rate shown in Figure 4 is the lower viscosity of the polymer-rich (matrix) phase. The polymer concentration at which the composition change path crosses the spinodal line (P_{cross}) is lower in the larger N case, which leads to the lower viscosity of the polymer-rich phase after the phase separation. Another reason is the higher volume fraction of the polymer lean phase. This is also brought about by the lower P_{cross}. The growth of Λ stopped faster in the P15N25 solution than in the P15N30 solution. In the former case, the polymer concentration of the polymer-rich phase is higher because of the higher P_{cross}, which leads to the shorter time up to the solidification of the polymer matrix phase attributed either to gelation or to glass transition.

Figure 6 shows the cross sections of the membranes. In three membranes, pore structures were almost isotropic and clear asymmetric structures were not observed. During the membrane formation, polymer and nonsolvent concentration gradients are formed along the membrane thickness direction because the solvent evaporates from the top surface. Therefore, the phase separation initially occurs near the top surface and then the structure is solidified. The zone, where the phase separation occurs, gradually moves to the deeper position in the membrane solution. If the structures are solidified in the similar stage of the phase separation in any positions, pore size does not vary with the membrane thickness direction. The isotropic pore structures obtained in this work may be explained by this process. The pore sizes increased with the increase of N. The interphase periodic distance Λ corresponds to the interpore distance.[22] The final constant Λ values obtained by the light-scattering measurement and the average interpore distances obtained from the SEM observation are compared in Table II. The data from the P15N35 solution were not listed in this table because the constant Λ was not obtained. Although the interpore distances are a little

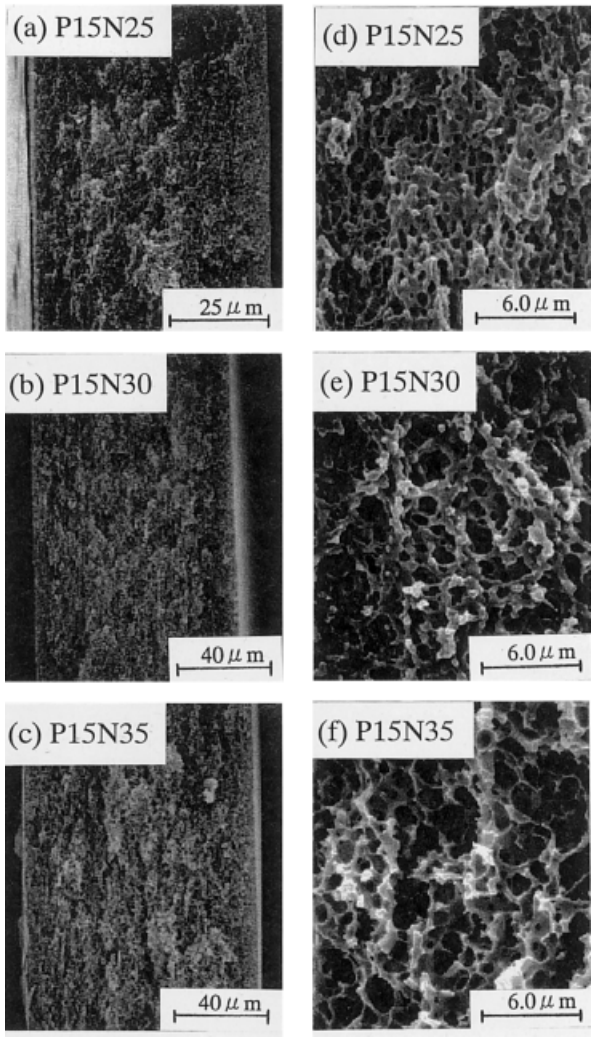

Figure 6 Cross sections of porous membranes. (a–c) Whole membrane cross sections. Left and right sides correspond to top and glass surfaces, respectively. (d–f) Structures in high magnification.

TABLE I
D_{app} and P_{cross} in Three Cases

Solution Composition	$D_{app} \times 10^2$ ($\mu m^2/s$)	P_{cross} (−)
P15N25	0.146	0.256
P15N30	0.896	0.217
P15N35	2.25	0.185

TABLE II
Comparison Between the Interphase Periodic Distance Λ and the Interpore Distance

Solution Composition	Interphase periodic distance, Λ (μm)	Interpore distance (μm)
P15N25	1.03	0.79
P15N30	1.44	1.26

smaller than the Λ values, the difference in both values is not remarkable.

CONCLUSIONS

The phase-separation mechanism by the dry-cast process was investigated by the light-scattering method. During the membrane-formation process, the maxima of the scattered light intensity were observed, which indicated that the phase separation occurred by the spinodal decomposition (SD) mechanism. In the early stage of SD, the apparent diffusion coefficient D_{app} was obtained. D_{app} increased with the increase of the nonsolvent amount in the cast solution.

The structure growth process was also investigated by the light-scattering method. The decrease of the nonsolvent amount brought about both the decrease of the growth rate and the sooner cessation of the structure growth.

The membrane cross sections were observed. The pore structures were isotopic rather than asymmetric. The average interpore distances obtained from the SEM observation roughly agreed with the final constant interphase periodic distances measured by the light-scattering method.

References

1. van de Witte, P.; Dijkstra, P. J.; van den Berg, J. W. A.; Feijen, J. J Membr Sci 1996, 117, 1.
2. Altena, F. W.; Smolders, C. A. Macromolecules 1982, 15, 1491.
3. Yilmaz, L.; McHugh, A. J. J Appl Polym Sci 1986, 31, 997.
4. Cheng, L.-P.; Dwan, A.-H.; Gryte, C. C. J Polym Sci Part B: Polym Phys 1994, 32, 1183.
5. Bulte, A. M. W.; Naafs, E. M.; van Eeten, F.; Mulder, M. H. V.; Smolders, C. A.; Strathmann, H. Polymer 1996, 37, 1647.
6. van de Witte, P.; Dijkstra, P. J.; van den Berg, J. W. A.; Feijen, J. J Polym Sci Part B: Polym Phys 1997, 35, 763.
7. Reuvers, A. J.; van den Berg, J. W. A.; Smolders, C. A. J Membr Sci 1987, 34, 45.
8. Tsay, C. S.; McHugh, A. J. J Polym Sci Part B: Polym Phys 1990, 28, 1327.
9. Radovanovic, P.; Thiel, S. W.; Hwang, S.-T. J Membr Sci 1992, 65, 213.
10. Shojaie, S. S.; Krantz, W. B.; Greenberg, A. R. J Membr Sci 1994, 94, 255.
11. Nunes, S. P.; Inoue, T. J Membr Sci 1996, 111, 93.
12. Barth, C.; Gongalves, M. C.; Pires, A. T. N.; Roeder, J.; Wolf, B. A. J Membr Sci 2000, 169, 287.
13. Schuhmacher, E.; Soldi, V.; Pires, A. T. N. J Membr Sci 2001, 184, 187.
14. Matsuyama, H.; Nushiguchi, M.; Kitamura, Y. J Appl Polym Sci 2000, 77, 776.
15. Flory, P. J. Principles of Polymer Chemistry; Cornell University Press: Ithaca, NY, 1953.
16. Mulder, M. H. V.; Smolders, C. A. J Membr Sci 1984, 17, 289.
17. Zielinski, J. M.; Duda, J. L. AIChE J 1992, 38, 405.
18. Hashimoto, T.; Kumaki, J.; Kawai, H. Macromolecules 1983, 16, 641.
19. Lal, J.; Bansil, R. Macromolecules 1991, 24, 290.
20. McGuire, K. S.; Laxminarayan, A.; Martula, D. S.; Lloyd, D. R. J Colloid Interface Sci 1996, 182, 46.
21. Matsuyama, H.; Teramoto, M.; Uesaka, T.; Goto, M.; Nakashio, F. J Membr Sci 1999, 152, 227.
22. Hashimoto, T.; Sasaki, K.; Kawai, H. Macromolecules 1984, 17, 2812.